Characterizing the Impact of SNR Heterogeneity on Time-of-Arrival based Localization Outage Probability

Sundar Aditya, *Member, IEEE*, Harpreet S. Dhillon, *Member, IEEE*, Andreas F. Molisch, *Fellow, IEEE*, R. Michael Buehrer, *Fellow, IEEE* and Hatim Behairy

***Abstract*—In localization, an outage occurs if the positioning mean squared error (MSE) exceeds a pre-defined threshold, ϵ_{th}. For time-of-arrival based localization, a key factor affecting the MSE is the relative positions of the anchors with respect to the target location. From a design point of view, characterizing the distribution of the MSE over an ensemble of anchor locations as seen from the perspective of a target is essential for providing probabilistic performance guarantees against outage. To solve this difficult problem, previous works have assumed all anchor-target links to have the same SNR (i.e., SNR homogeneity), which neglects the impact of link distance variation on the SNR and the positioning error; for instance, under an inverse square law pathloss model, the outage probability can differ by orders of magnitude when compared to the homogeneous SNR assumption. In this paper, we derive an approximate expression for the MSE distribution under an inverse square law pathloss model when the anchors are uniformly distributed around a target. Through simulations, we verify that our approximation can be used to estimate the number of anchors needed so that the outage probability is below 1%.**

***Index Terms*—Localization outage probability; Time-of-arrival (ToA) based localization; Squared position error bound (SPEB); SNR heterogeneity; Geometric dilution of precision (GDOP); Cramer-Rao Lower Bound (CRLB); Binomial point process (BPP); Constrained moment matching.**

I. Introduction

In recent years, the number of applications requiring accurate position information has grown steadily; from navigation for autonomous vehicles [1] to crowd-sensing [2], location-based advertising [3] and virtual reality [4], to name a few. On a two-dimensional surface, a target can be localized if its distance (also known as *range*) to at least three fixed reference points, called anchors, is known (see Fig. 1). For wireless systems, ranges can be estimated from the time-of-arrival (ToA) of a *ranging signal*[1] and for wideband systems in particular, ToA-based localization is especially attractive, since the finer time resolution due to the large bandwidth improves the accuracy of the range estimates [5], thereby resulting in accurate location estimates.

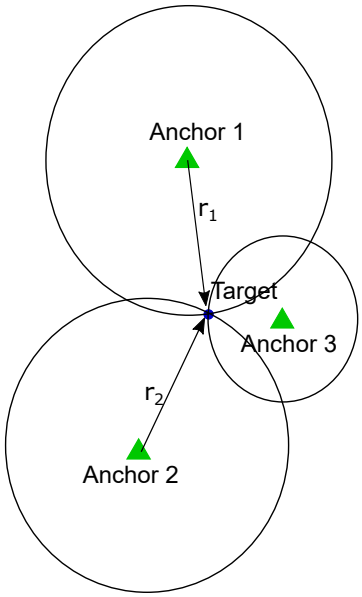

Fig. 1: ToA based localization: Each distance (range) estimate constrains the target to lie on a circle centered at the corresponding anchor, whose radius equals the range. The intersection of three or more such circles provides an unambiguous solution for the target location in $\mathbb{R}^2$.

While the principle behind ToA-based localization is fairly straightforward, a variety of operating conditions and propagation phenomena, such as noise, interference, multipath, blocking, target mobility etc. render the task of designing a localization network challenging. In order to provide a reliable quality of service in terms of accuracy (e.g., an error of at most 50m at least 90% of the time, as mandated by the the E911 standard [6]), it is important to characterize the probability distribution of the localization mean squared error (MSE) over an ensemble of operating conditions, especially for safety critical applications like autonomous vehicles or E911 emergency services. The MSE is a function of the anchor locations relative to the target, the transmit powers, the propagation environment as well as the choice of ranging and localization algorithms. For localization algorithms that

S. Aditya was with the University of Southern California, Los Angeles, CA 90089 USA. He is now with NYU WIRELESS, New York University Tandon School of Engineering, Brooklyn, NY 11201 USA (e-mail: sundar.aditya@nyu.edu)

H. S. Dhillon and R. M. Buehrer are with Wireless@VT, Bradley Dept. of Electrical and Computer Engineering, Virginia Tech., Blacksburg, VA 24061 USA (e-mail: {hdhillon, buehrer}@vt.edu).

A. F. Molisch is with Wireless Devices and Systems (WiDeS), Ming Hsieh Dept. of Electrical Engineering, University of Southern California, Los Angeles, CA 90089 USA (e-mail: molisch@usc.edu).

H. Behairy is with King Abdulaziz City for Science and Technology, P. O. Box 6086, Riyadh 11442, Saudi Arabia (e-mail: hbehairy@kacst.edu.sa)
Revised: November 25, 2018.

This work was supported by KACST under grant number 33-878.

[1]This requires the targets and anchors to be synchronized.

return unbiased[2] estimates of the target location, the MSE is bounded below by the squared position error bound (SPEB) [7], [8]. Unlike the MSE, the SPEB does not depend on a specific localization algorithm and is a function of the anchor locations relative to the target, among other things. As a result, it is well-suited as a metric to analyze the impact of the anchor geometry around a target on the MSE. If the SPEB exceeds a pre-defined threshold, $\epsilon_{\rm th}$, then the target is said to be in *outage*. Over an ensemble of anchor locations as seen from the perspective of a target, the SPEB (and the MSE, as well) is a random variable and characterizing its complementary cumulative distribution function (ccdf) in closed-form (i.e., $\mathbb{P}(\text{SPEB} > u)$, as a function of u) is important from a design perspective, as it can be used to determine a deployment of anchors that can guarantee an outage probability of at most $p_{\rm out}$[3] across an ensemble of target locations, assuming spatial stationarity and ergodicity. Given N anchors within communication range from the target, a natural model for capturing the randomness in the anchor locations is the well-known binomial point process (BPP) [9, Chap. 2], in which the anchors are distributed independently and uniformly over an annular region centered at the target. In this paper, we attempt to derive a closed-form expression for the SPEB ccdf for such an anchor model. Our approach is summarized below.

A. Methodology

- For a given target, we assume that the anchors that are within its communication range are distributed according to a BPP over an annular region centered at the target. For this setup, we model the SNR heterogeneity across different anchor-target links using a pathloss model. As a result, the SPEB metric is a function of the anchor distances and angular positions, relative to the target.
- Given N anchors within communication range from the target, we rearrange the SPEB expression and reduce it in terms of the product of two random variables, X_N and Y_N. While X_N depends only on the anchor distances, Y_N depends on both the distances and angular positions of the anchors. In particular, Y_N and X_N are statistically dependent.
- We then proceed to demonstrate that the conditional distribution of Y_N, given X_N, is difficult to characterize in closed form. Hence, through *constrained moment matching*, we derive an approximation for Y_N, denoted by V_N, which depends only on the angular positions of the anchors and has the same mean as Y_N. In particular, X_N and V_N are statistically independent.
- Consequently, the SPEB can be approximated in terms of the product of independent random variables, X_N and V_N, and we derive a closed-form expression for the ccdf of this approximation (see Theorem 1 in Section III), which is the key result of this paper.
- Through simulations, we verify that the derived SPEB ccdf accurately estimates the true ccdf. Thus, from a design perspective, our contribution is useful in determining the number of anchors required to satisfy $p_{\rm out} \leq \delta$, for any $\delta \in (0, 1)$. We also show that the accuracy of our approach is superior to that of other approaches that ignore SNR heterogeneity, which serves to highlight the impact of SNR heterogeneity on the SPEB (and consequently, the MSE) distribution.

[2]An estimate $\hat{\mathbf{p}}$ of a target location $\mathbf{p}$ is said to be unbiased if $\mathbb{E}[\hat{\mathbf{p}}] = \mathbf{p}$.

[3]For a given error threshold, $\epsilon_{\rm th}$, an outage probability of at most $p_{\rm out}$ can be guaranteed if and only if the condition $\mathbb{P}(\text{SPEB} > \epsilon_{\rm th}) \leq p_{\rm out}$ is satisfied, which poses a constraint on the shape of the SPEB ccdf.

B. Related Work

There have been a number of recent works that have focused on the impact of anchor geometry on the localization error performance; specifically, for the SPEB metric, the impact of the target being situated within the convex hull of the anchors was investigated in [10], while scaling laws with respect to the number of anchors within communication range were derived in [11]. A related, but simpler metric, known as the geometric dilution of precision (GDOP) has been studied extensively for the BPP anchor model. The GDOP corresponds to a special case of the SPEB when all the anchor-target links have the same SNR. The asymptotic distribution of the GDOP, as the number of anchors approaches infinity, was derived using U-statistics in [12]. For the more realistic case of a finite number of anchors, the max-angle metric was proposed and analyzed in [13] and shown to be correlated to the GDOP. An approximate GDOP distribution was presented in [14], using the order statistics of the inter-node angles, while the *exact* GDOP distribution was characterized in [15]. To the best of our knowledge, ours is the first work to consider the more realistic scenario where the anchor-target links may have different SNRs (due to the anchors being situated at different distances from the target), which increases the difficulty of the problem considerably, as highlighted in Section II.

C. Notation

Throughout this work, bold lower case letters are used for deterministic vectors. In particular, $\mathbf{1}$ denotes the all-one vector. Uppercase letters in serif font are used for scalar random variables (e.g., X), while random vectors are underlined and similarly represented (e.g., $\underline{\mathsf{X}}$). For square matrices, the trace and inverse operators are respectively denoted by $\mathrm{tr}(\cdot)$ and $(\cdot)^{-1}$. $\mathbb{R}$ represents the real numbers, $\mathbb{C}$ the complex numbers, $i \in \mathbb{C}$ the imaginary unit, and $\mathrm{Im}(z)$ the imaginary part of $z \in \mathbb{C}$. For random variables X and Y, $f_{\mathsf{X}}(\cdot)$, $\overline{F}_{\mathsf{X}}(\cdot)$ and $\varphi_{\mathsf{X}}(\cdot)$ denote the marginal probability density function (pdf), the marginal ccdf and the characteristic function of X, respectively, while $\overline{F}_{\mathsf{X}|\mathsf{Y}}(.|y)$ denotes the conditional ccdf of X, given $\mathsf{Y} = y$. $\mathbb{P}(.)$ denotes the probability measure, while $\mathbb{E}_{\mathsf{X}}[.]$ denotes the expectation operator over the distribution of X. A real, parametrized function $h : \mathbb{R} \to \mathbb{R}$, with argument t and parameters given by a vector, $\mathbf{a}$, is denoted by $h(t; \mathbf{a})$. For $x \in \mathbb{R}$, the sine and cosine integrals, denoted by $\mathrm{Si}(x)$ and $\mathrm{Ci}(x)$, respectively, are defined as follows:

$$\mathrm{Si}(x) = \int_0^x \frac{\sin t}{t}\, \mathrm{d}t, \tag{1}$$

$$\mathrm{Ci}(x) = -\int_{x}^{\infty} \frac{\cos t}{t}\ \mathrm{d}t. \tag{2}$$

$\mathbb{1}(\cdot)$ denotes the indicator function and finally, the function $\mathrm{H} : \mathbb{R} \to \mathbb{C}$ is defined as follows:

$$\mathrm{H}(x) := \mathrm{Si}(x) - i\mathrm{Ci}(x),\ x \in \mathbb{R}. \tag{3}$$

D. Organization

This paper is divided into five sections. The system model is described in Section II, where the anchors are modeled by a BPP over an annular region surrounding the target, and a distance-dependent pathloss model is assumed for the SNRs of the anchor-target links. Under these conditions, we illustrate the difficulty of characterizing the SPEB distribution in Section III, which motivates the derivation of a tractable approximation for the SPEB ccdf later on in the same section. In Section IV, we compare the accuracy of our approach with other bounds and approximations that do not consider SNR heterogeneity. Finally, Section V concludes the paper.

II. System Model

Consider a target situated in $\mathbb{R}^2$ that needs to be localized. Since we are interested in the anchor geometry relative to the target, we can assume, without loss of generality, that the target is situated at the origin, $\mathbf{o}$. Centered at the target, consider $N \geq 3$ anchors deployed according to a BPP[4] over an annular region from $d_{\min}$ to $d_{\max}$ ($d_{\max} > d_{\min} > 0$)[5], denoted by $\mathcal{A}_{\mathbf{o}}(d_{\min}, d_{\max})$, and let (R_k, Θ_k) denote the location of the k-th anchor in polar coordinates ($\mathsf{R}_k \in [d_{\min}, d_{\max}],\ \Theta_k \in [0, 2\pi);\ k = 1, \cdots, N$). Let $s(t)$, having Fourier transform $S(f)$, denote the ranging signal transmitted by the anchors[6] and let $y(t; \mathsf{R}_k, \Theta_k)$ denote the signal received from the k-th anchor, which can be modeled as a superposition of a number of multipath components (MPCs) in the following manner:

$$y(t; \mathsf{R}_k, \Theta_k) = \sum_{l=1}^{L(\mathsf{R}_k, \Theta_k)} \alpha_l(\mathsf{R}_k, \Theta_k) s(t - \tau_l(\mathsf{R}_k, \Theta_k)) + \eta_k(t); \quad k \in \{1, \cdots, N\}, \tag{4}$$

where the location-dependent quantities $L(\mathsf{R}_k, \Theta_k)$, $\alpha_l(\mathsf{R}_k, \Theta_k) \in \mathbb{C}$ and $\tau_l(\mathsf{R}_k, \Theta_k) \in \mathbb{R}$ respectively denote the number of observed MPCs, the complex amplitude of the l-th MPC and its ToA. $\eta_k(t)$ is the measurement noise, which is modeled as a zero-mean complex Gaussian random process, having a power spectral density of N_0. We assume that line-of-sight exists from the target to all the anchors. Hence, the first arriving MPC from each anchor corresponds to the direct path (DP) and depends on the anchor position as follows:

$$\tau_1(\mathsf{R}_k, \Theta_k) = \tau_1(\mathsf{R}_k) = \frac{\mathsf{R}_k}{c},\ k \in \{1, \cdots, N\}, \tag{5}$$

where c denotes the speed of light in free space. The other MPCs are known as indirect paths (IPs) and we assume no prior knowledge of their statistics. Under these conditions, the MSE of an unbiased estimate of the target location can be bounded using the Cramer-Rao lower bound (CRLB) [7], [8], as follows:

$$\mathrm{MSE} \geq \mathrm{tr}\left(\left(\sum_{k=1}^{N} \mu(\mathsf{R}_k, \Theta_k)\mathbf{u}(\Theta_k)\mathbf{u}(\Theta_k)^T\right)^{-1}\right) \tag{6}$$

$$:= \mathsf{S}(\underline{\mathsf{R}}^{(N)}, \underline{\Theta}^{(N)}), \tag{7}$$

$$\text{where } \underline{\mathsf{R}}^{(N)} = [\mathsf{R}_1,\ \cdots,\ \mathsf{R}_N]^T, \tag{8}$$

$$\underline{\Theta}^{(N)} = [\Theta_1,\ \cdots,\ \Theta_N]^T, \tag{9}$$

$$\mu(\mathsf{R}_k, \Theta_k) = \frac{8\pi^2\beta^2(1 - \chi(\mathsf{R}_k, \Theta_k))\gamma(\mathsf{R}_k, \Theta_k)}{c^2}, \tag{10}$$

$$\gamma(\mathsf{R}_k, \Theta_k) = \frac{|\alpha_1(\mathsf{R}_k, \Theta_k)|^2}{N_0} \int_{-\infty}^{\infty} |s(t)|^2\ \mathrm{d}t, \tag{11}$$

$$\beta = \sqrt{\left(\int_{-\infty}^{\infty} f^2 |S(f)|^2 \mathrm{d}f\right) \Big/ \left(\int_{-\infty}^{\infty} |S(f)|^2 \mathrm{d}f\right)}, \tag{12}$$

$$\text{and } \mathbf{u}(\Theta_k) = [\cos(\Theta_k)\ \ \sin(\Theta_k)]^T. \tag{13}$$

$\mathsf{S}(\underline{\mathsf{R}}^{(N)}, \underline{\Theta}^{(N)})$ is commonly known as the squared position error bound (SPEB) [7], [8] in localization terminology. The term $\mu(\mathsf{R}_k, \Theta_k)$ is referred to as the *ranging information intensity* (RII) from the k-th anchor and is a measure of the ranging accuracy associated with the k-th anchor[7]. It is a function of the DP SNR, $\gamma(\mathsf{R}_k, \Theta_k)$, the *effective bandwith*, β, and the path overlap factor, $\chi(\mathsf{R}_k, \Theta_k) \in [0, 1]$, which determines the extent of overlap between the DP and subsequent MPCs, due to finite bandwidth[8].

Remark 1. *Since $\underline{\mathsf{R}}^{(N)}$ and $\underline{\Theta}^{(N)}$ are random vectors, $\mathsf{S}(\underline{\mathsf{R}}^{(N)}, \underline{\Theta}^{(N)})$ is a random variable. Moreover, the inequality in (6) holds for each realization of $\underline{\mathsf{R}}^{(N)}$ and $\underline{\Theta}^{(N)}$. Hence, over an ensemble of anchor locations relative to the target, the MSE random variable stochastically dominates $\mathsf{S}(\underline{\mathsf{R}}^{(N)}, \underline{\Theta}^{(N)})$.*

For simplicity, we assume $\chi(\mathsf{R}_k, \Theta_k) = 0$ for all k, which corresponds to the case where the DP does not overlap with any other MPC, thereby resulting in the most accurate estimate of R_k. Furthermore, $\gamma(\mathsf{R}_k, \Theta_k)$ is a function of the DP attenuation, $|\alpha_1(\mathsf{R}_k, \Theta_k)|^2$, for which the following *pathloss* model is assumed:

$$|\alpha_1(\mathsf{R}_k, \Theta_k)|^2 = |\alpha_1(\mathsf{R}_k)|^2 = (d_{\min}/\mathsf{R}_k)^2. \tag{14}$$

[4]Typically, the number of anchors, N, is also a random variable, often modeled as having a Poisson distribution. Together with the randomness in the anchor locations, this corresponds to the well-known homogeneous Poisson point process (PPP), which has been used to analyze the localization performance of a variety of wireless networks [16]–[20]. Hence, the results presented in this paper for the BPP anchor model can be readily extended for the PPP case by averaging over the distribution of N.

[5]$d_{\min}$ denotes the distance beyond which the far-field assumption holds while $d_{\max}$ denotes the distance beyond which the ranging signal is too weak to be detected by the target.

[6]We assume that the anchors coordinate their transmissions to avoid interference at the target. As a result, ToA/range estimation is noise-limited.

[7]$1/\mu(\mathsf{R}_k, \Theta_k)$ is the CRLB for an unbiased estimate of R_k [5].

[8]The expression for $\chi(\mathsf{R}_k, \Theta_k)$ can be found in [8].

Remark 2. *For anchors having line-of-sight to the target, the inverse-square law pathloss model in (14) is a reasonable assumption for the DP component if there is zero path overlap, which, in turn, can be assumed when $d_{\max} < d_{\text{break}}$, where d_{break} denotes the breakpoint distance associated with the ground reflection [21], since zero overlap between the DP and the ground-reflected path can rarely be achieved.*

Apart from the RIIs, which depend primarily on the ranges, $\mathsf{S}(\underline{\mathsf{R}}^{(N)}, \underline{\Theta}^{(N)})$ also depends on the angular geometry of the anchors, which is captured in (6) by the outer product $\mathbf{u}(\Theta_k)\mathbf{u}(\Theta_k)^T$, where $\mathbf{u}(\Theta_k)$ is the unit vector in the direction of the k-th anchor. In summary, the k-th term in the summation in (6) represents the contribution of the k-th anchor to $\mathsf{S}(\underline{\mathsf{R}}^{(N)}, \underline{\Theta}^{(N)})$. From (6)-(14), $\mathsf{S}(\underline{\mathsf{R}}^{(N)}, \underline{\Theta}^{(N)})$ can be expressed as follows:

$$\mathsf{S}(\underline{\mathsf{R}}^{(N)}, \underline{\Theta}^{(N)}) = \frac{\sum_{k=1}^{N} \mathsf{R}_k^{-2}}{T_{\text{s}} \sum_{j=1}^{N-1} \sum_{k=j+1}^{N} \mathsf{R}_j^{-2}\mathsf{R}_k^{-2} \sin^2(\Theta_j - \Theta_k)}, \tag{15}$$

$$\text{where } T_{\text{s}} = \frac{8\pi^2\beta^2 d_{\min}^2}{N_0 c^2} \int_{-\infty}^{\infty} |s(t)|^2 \, \mathrm{d}t. \tag{16}$$

Since $\mathsf{S}(\underline{\mathsf{R}}^{(N)}, \underline{\Theta}^{(N)})$ does not depend on any particular positioning algorithm, it is well-suited as a metric to analyze the impact of anchor geometry on the MSE. Moreover, many positioning algorithms have been proposed in recent years that have been shown to satisfy (6) with equality [22]–[25]. Hence, for the remainder of this paper, we assume that the MSE is identical to $\mathsf{S}(\underline{\mathsf{R}}^{(N)}, \underline{\Theta}^{(N)})$. In the next section, we attempt to characterize the ccdf of $\mathsf{S}(\underline{\mathsf{R}}^{(N)}, \underline{\Theta}^{(N)})$ in closed form.

III. Characterizing SPEB distribution

A. A Special Case: SNR Homogeneity

For the special case when all the anchors are at the same distance R from the target (i.e., all links have the same SNR), $\mathsf{S}(\underline{\mathsf{R}}^{(N)}, \underline{\Theta}^{(N)})$ reduces to another well-known metric called the Geometric Dilution of Precision (GDOP), which is denoted by $\mathsf{G}(\mathsf{R}, \underline{\Theta}^{(N)})$ and has the following expression[9]:

$$\begin{aligned}\mathsf{S}(\mathsf{R}\mathbf{1}, \underline{\Theta}^{(N)}) &:= \mathsf{G}(\mathsf{R}, \underline{\Theta}^{(N)}) \\ &= \frac{N\mathsf{R}^2}{T_{\text{s}} \sum_{j=1}^{N-1} \sum_{k=j+1}^{N} \sin^2(\Theta_j - \Theta_k)} \\ &\overset{(a)}{=} \frac{1}{T_{\text{s}}} \frac{4\mathsf{R}^2}{N\mathsf{W}_N},\end{aligned} \tag{17}$$

$$\text{where } \mathsf{W}_N = 1 - \frac{1}{N^2}\left[\left(\sum_{k=1}^{N} \cos 2\Theta_k\right)^2 + \left(\sum_{k=1}^{N} \sin 2\Theta_k\right)^2\right]. \tag{18}$$

[9]Technically, the GDOP is defined as the square root of $\mathsf{G}(\mathsf{R}, \underline{\Theta}^{(N)})$ [26] and thus, has the units of distance. However, in order to have a fair comparison with $\mathsf{S}(\underline{\mathsf{R}}^{(N)}, \underline{\Theta}^{(N)})$ (which has units of distance-squared), we slightly abuse the notation and refer to $\mathsf{G}(\mathsf{R}, \underline{\Theta}^{(N)})$ as the GDOP in this work.

For the derivation of (a) in (17), the reader is referred to [27, Lemma 1] and [28, Prop. 3], where a more general result is proved.

From (17), it is evident that $\mathsf{G}(\mathsf{R}, \underline{\Theta}^{(N)})$ can be decomposed in terms of the radial and the azimuthal (or angular) geometry of the anchor locations through the terms R^2 and W_N, respectively. Since the radial contribution (i.e., R^2) merely acts as a scaling term, $\mathsf{G}(\mathsf{R}, \underline{\Theta}^{(N)})$ essentially captures the relationship between the MSE and the azimuthal geometry of the anchor locations. Since the radial and azimuthal coordinates are independent random variables for the BPP anchor model, the ccdf of $\mathsf{G}(\mathsf{R}, \underline{\Theta}^{(N)})$, denoted by $\overline{F}_{\mathsf{G}_N}(\cdot)$, can be evaluated as follows:

$$\begin{aligned}\overline{F}_{\mathsf{G}_N}(u) &= \mathbb{P}(\mathsf{G}(\mathsf{R}, \underline{\Theta}^{(N)}) > u) \\ &= 1 - \mathbb{E}_{\mathsf{R}}\left[\overline{F}_{\mathsf{W}_N}\left(\frac{4\mathsf{R}^2}{T_{\text{s}} N u}\right)\right],\end{aligned} \tag{19}$$

where the ccdf of W_N has the following expression [15],

$$\overline{F}_{\mathsf{W}_N}(u) = \begin{cases} 1, \ u < 0 \\ N\sqrt{1-u} \displaystyle\int_0^{\infty} J_1\left(N\sqrt{1-u}\ y\right) \ (J_0(y))^N \mathrm{d}y, \\ \qquad\qquad\qquad\qquad u \in [0,1] \\ 0, \ u > 1, \end{cases} \tag{20}$$

with $J_0(.)$ and $J_1(.)$ denoting the zeroth and first order Bessel functions, respectively, while the pdf of R is given by

$$f_{\mathsf{R}}(r) = \frac{2r}{d_{\max}^2 - d_{\min}^2} \mathbb{1}(r \in [d_{\min}, d_{\max}]). \tag{21}$$

In contrast to $\mathsf{G}(\mathsf{R}, \underline{\Theta}^{(N)})$, $\mathsf{S}(\underline{\mathsf{R}}^{(N)}, \underline{\Theta}^{(N)})$ cannot, in general, be decomposed in terms of the radial and azimuthal geometries of the anchor locations since the $\sin^2(\cdot)$ terms in the denominator of (15) are weighted differently when the anchors are not constrained to be equidistant from the target[10]. As a result, a statistical characterization of $\mathsf{S}(\underline{\mathsf{R}}^{(N)}, \underline{\Theta}^{(N)})$ is challenging. Hence, we formulate a tractable approximation for $\mathsf{S}(\underline{\mathsf{R}}^{(N)}, \underline{\Theta}^{(N)})$ in the following subsection.

B. The General Case: SNR Heterogeneity

Although $\mathsf{S}(\underline{\mathsf{R}}^{(N)}, \underline{\Theta}^{(N)})$ cannot, in general, be decomposed in terms of the radial and azimuthal geometries of the anchor locations, a partial decomposition can be obtained as shown in the lemma below:

Lemma 1. *The expression for $\mathsf{S}(\underline{\mathsf{R}}^{(N)}, \underline{\Theta}^{(N)})$ in (15) can be re-written as follows:*

$$\mathsf{S}(\underline{\mathsf{R}}^{(N)}, \underline{\Theta}^{(N)}) = \frac{4}{T_{\text{s}} \mathsf{X}_N \mathsf{Y}_N}, \tag{22}$$

[10]Just as it is generally not possible to represent an expression like $a_1x_1 + \cdots + a_Mx_M$ as $h_1(a_1, \cdots, a_M)h_2(x_1, \cdots, x_M)$ (i.e., as a product of scalar-valued real functions $h_1(\cdot)$ and $h_2(\cdot)$) when a_i and x_i $(i = 1, \cdots, M)$ can take arbitrary real values, the denominator of (15) cannot, in general, be expressed as $\mathsf{S}_1(\underline{\mathsf{R}}^{(N)})\mathsf{S}_2(\underline{\Theta}^{(N)})$, for some choice of $\mathsf{S}_1(\cdot)$ and $\mathsf{S}_2(\cdot)$.

$$\textit{where } \mathsf{X}_N = \sum_{k=1}^{N} \mathsf{A}_k, \tag{23}$$

$$\mathsf{A}_k = \mathsf{R}_k^{-2}, \tag{24}$$

$$\mathsf{Y}_N = 1 - \left(\sum_{k=1}^{N} \mathsf{B}_{k,N} \cos 2\Theta_k\right)^2 - \left(\sum_{k=1}^{N} \mathsf{B}_{k,N} \sin 2\Theta_k\right)^2, \tag{25}$$

$$\textit{and } \mathsf{B}_{k,N} = \frac{\mathsf{A}_k}{\mathsf{X}_N},\ k = 1, \cdots, N. \tag{26}$$

Proof: See [27, Lemma 1] or [28, Prop. 3]. ∎

While X_N depends only on $\underline{\mathsf{R}}^{(N)}$, Y_N is a function of both $\underline{\mathsf{R}}^{(N)}$ and $\underline{\Theta}^{(N)}$. Moreover, since Y_N is a function of X_N, the two random variables are statistically dependent. Let $\overline{F}_{\mathsf{S}_N}(\cdot)$ denote the ccdf of $\mathsf{S}(\underline{\mathsf{R}}^{(N)}, \underline{\Theta}^{(N)})$, which can be expressed as follows:

$$\begin{aligned}\overline{F}_{\mathsf{S}_N}(u) &= \mathbb{P}(\mathsf{S}(\underline{\mathsf{R}}^{(N)}, \underline{\Theta}^{(N)}) > u) \\ &= \mathbb{P}\left(\mathsf{X}_N \mathsf{Y}_N \leq \frac{4}{uT_{\mathrm{s}}}\right) \\ &= 1 - \mathbb{E}_{\mathsf{X}_N}\left[\overline{F}_{\mathsf{Y}_N|\mathsf{X}_N}\left(\frac{4}{uxT_{\mathrm{s}}}\middle| x\right)\right]. \end{aligned} \tag{27}$$

We now attempt to characterize the marginal distribution of X_N and the conditional distribution Y_N, given X_N.

Lemma 2. *The characteristic function of X_N is given by:*

$$\varphi_{\mathsf{X}_N}(t) = (\varphi_{\mathsf{A}_1}(t))^N, \tag{28}$$

$$\begin{aligned}\textit{where } \varphi_{\mathsf{A}_1}(t) = \frac{1}{d_{\max}^2 - d_{\min}^2} &\left[d_{\max}^2 \exp\left(i\frac{t}{d_{\max}^2}\right)\right. \\ &- d_{\min}^2 \exp\left(i\frac{t}{d_{\min}^2}\right) + t\mathrm{H}\left(\frac{t}{d_{\max}^2}\right) \\ &\left. - t\mathrm{H}\left(\frac{t}{d_{\min}^2}\right)\right], \end{aligned} \tag{29}$$

and $\mathrm{H}(\cdot)$ is given by (3).

Proof: See Appendix A. ∎

From $\varphi_{\mathsf{X}_N}(t)$, the ccdf of X_N can be evaluated as follows [29]:

$$\overline{F}_{\mathsf{X}_N}(x) = \frac{1}{2} + \frac{1}{\pi}\int_0^\infty \frac{\mathrm{Im}\{\exp(-itx)\varphi_{\mathsf{X}_N}(t)\}}{t}\,\mathrm{d}t. \tag{30}$$

Remark 3. *We have chosen to characterize X_N by its ccdf instead of its pdf, since the ccdf can be obtained from the characteristic function by evaluating a single integral, which is computationally less intensive than the double integral required to obtain the pdf. Since X_N is non-negative, the expected value of $h(\mathsf{X}_N)$, for a differentiable real function $h(\cdot)$, can be expressed in terms of $\overline{F}_{\mathsf{X}_N}(\cdot)$ by considering the following expression:*

$$\begin{aligned} h(\mathsf{X}_N) &= h(0) + \int_0^{\mathsf{X}_N} h'(u)\mathrm{d}u \\ &= h(0) + \int_0^\infty h'(u)\mathbb{1}(\mathsf{X}_N > u)\mathrm{d}u, \end{aligned} \tag{31}$$

where $h'(\cdot)$ denotes the derivative of $h(\cdot)$. Applying the expectation operator on both sides of (31), we obtain

$$\mathbb{E}[h(\mathsf{X}_N)] = h(0) + \int_0^\infty h'(u)\overline{F}_{\mathsf{X}_N}(u)\mathrm{d}u. \tag{32}$$

While the marginal distribution of X_N is fairly tractable, as it is the sum of N independent and identically distributed (iid) random variables, the same cannot be said of $\overline{F}_{\mathsf{Y}_N|\mathsf{X}_N}(\cdot|x)$. To illustrate this, consider the expression for Y_N, given $\mathsf{X}_N = x$:

$$\begin{aligned}\mathsf{Y}_N = 1 &- \frac{1}{x^2}\sum_{k=1}^{N}\mathsf{A}_k^2 \\ &- \frac{2}{x^2}\sum_{j=1}^{N-1}\sum_{k=j+1}^{N}\mathsf{A}_j\mathsf{A}_k(\cos 2\Theta_j \cos 2\Theta_k + \sin 2\Theta_j \sin 2\Theta_k). \end{aligned} \tag{33}$$

Let $\underline{\mathsf{A}}^{(N)} = [\mathsf{A}_1, \cdots, \mathsf{A}_N]^T$. Given $\mathsf{X}_N = x$, it is easily seen from (23) and (33) that $\underline{\mathsf{A}}^{(N)}$ is a vector of identically distributed, but *not independent* random variables. Hence, in order to characterize $\overline{F}_{\mathsf{Y}_N|\mathsf{X}_N}(\cdot|x)$, the conditional joint distribution of $\underline{\mathsf{A}}^{(N)}$, given $\mathsf{X}_N = x$, is required, which is not easy to express in closed form. From (25), it is clear that the dependence between X_N and Y_N is induced by the collection of random variables, $\{\mathsf{B}_{k,N} : k = 1, \cdots, N\}$. For the sake of tractability, we remove this dependence by assuming $\mathsf{B}_{k,N} \approx m$, for some $m \geq 0$; furthermore, to obtain a random variable whose second-order statistics match that of Y_N, we approximate Y_N as follows:

Approximation 1. $\mathsf{Y}_N \approx \mathsf{V}_N$, *where*

$$\mathsf{V}_N := v\left(1 - m^2\left[\left(\sum_{k=1}^{N}\cos 2\Theta_k\right)^2 + \left(\sum_{k=1}^{N}\sin 2\Theta_k\right)^2\right]\right). \tag{34}$$

The parametric form for V_N in (34) is based on the expression for Y_N given by (25) and the values of the parameters, v and m, can be determined by moment matching with Y_N. From (34), the mean and variance of V_N are given by:

$$\mathbb{E}[\mathsf{V}_N] = v(1 - m^2 N). \tag{35}$$

$$\begin{aligned}\sigma_{\mathsf{V}_N}^2 &= \mathbb{E}[(\mathsf{V}_N - \mathbb{E}[\mathsf{V}_N])^2] \\ &= 2\binom{N}{2}v^2m^4, \end{aligned} \tag{36}$$

where (35) follows as a result of $\underline{\Theta}^{(N)}$ being an iid uniform random vector over $[0, 2\pi)$. Equating $\mathbb{E}[\mathsf{V}_N]$ and $\sigma_{\mathsf{V}_N}^2$ with the corresponding quantities for Y_N, i.e., $\mathbb{E}[\mathsf{Y}_N]$ and $\sigma_{\mathsf{Y}_N}^2$, we obtain the following expressions for m and v:

$$m = \frac{1}{\sqrt{v}}\left(\frac{\sigma_{\mathsf{Y}_N}^2}{N(N-1)}\right)^{1/4}, \tag{37}$$

$$v = \mathbb{E}[\mathsf{Y}_N] + N\sqrt{\frac{\sigma_{\mathsf{Y}_N}^2}{N(N-1)}}. \tag{38}$$

However, since Y_N is non-negative, a similar requirement on V_N imposes the following constraint on m:

$$\mathsf{V}_N \geq 0,$$

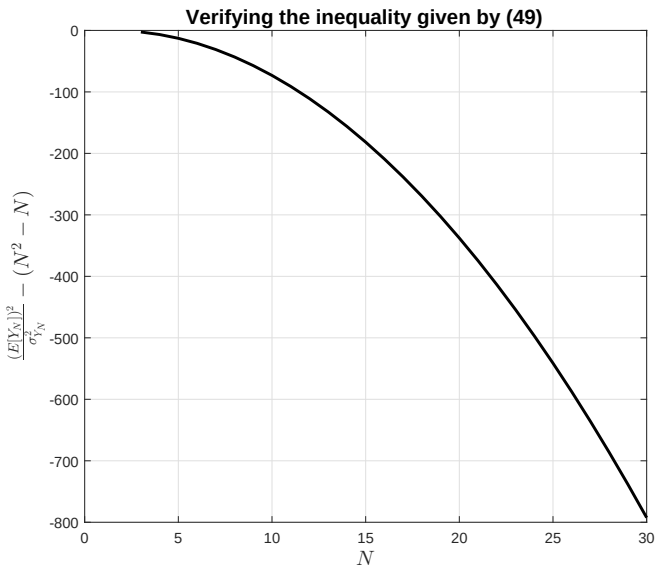

Fig. 2: Since (41) is not satisfied, it follows that (37), (38) and (40) cannot be satisfied simultaneously. The values of $\mathbb{E}[\mathsf{Y}_N]$ and $\sigma^2_{\mathsf{Y}_N}$ were obtained empirically from 10^6 samples. For a closed-form characterization of $\mathbb{E}[\mathsf{Y}_N]$, see Lemma 3.

$$\implies \quad m^2 \max_{\underline{\Theta}^{(N)}} \underbrace{\left[\left(\sum_{k=1}^{N} \cos 2\Theta_k\right)^2 + \left(\sum_{k=1}^{N} \sin 2\Theta_k\right)^2\right]}_{\text{squared distance of } N\text{-step random walk}} \leq 1. \tag{39}$$

The term in square parentheses in (39) can be interpreted as the squared distance of an N-step two-dimensional random walk with unit step size; thus, it has a maximum value of N^2, obtained when all the steps are in the same direction (i.e., $\Theta_k = \Theta$, for all k). Therefore,

$$0 \leq m \leq 1/N. \tag{40}$$

From (37) and (38), the upper bound on m given by (40) reduces to the following equivalent constraint on the second-order statistics of Y_N:

$$\frac{(\mathbb{E}[\mathsf{Y}_N])^2}{\sigma^2_{\mathsf{Y}_N}} - (N^2 - N) \geq 0. \tag{41}$$

However, from Fig. 2, it can be seen that (41) is not satisfied for any $N \geq 3$; in fact, the expression on the left-hand side of (41) becomes increasingly negative as N increases. Thus, it follows that (37), (38) and (40) are not satisfied simultaneously. In particular, the expression for m in (37) is greater than $1/N$. As a result, we optimize for the values of m and v in the following manner:

$$\min_{m,v} \ |\sigma^2_{\mathsf{Y}_N} - \sigma^2_{\mathsf{V}_N}| \tag{42}$$

$$\text{subject to } (40),$$

$$\mathbb{E}[\mathsf{Y}_N] = \mathbb{E}[\mathsf{V}_N], \tag{43}$$

where the above optimization problem can be viewed as *constrained moment matching*, due to the non-negativity constraint on V_N imposed by (40). From (43) and (35), the objective function in (42) can be represented in terms of a single parameter, m, as follows:

$$\left|\sigma_{\mathsf{Y}_N^2} - N(N-1)(\mathbb{E}[\mathsf{Y}_N])^2 \frac{m^4}{(1-m^2N)^2}\right| \tag{44}$$

For $m > 0$, the expression in (44) is initially a monotonically decreasing function of m and attains a minimum value of zero, for m given by (37). However, as observed previously, this value of m does not lie in the feasible region, $0 \leq m \leq 1/N$. Consequently, the minimum value of (44) over $m \in [0, 1/N]$ is attained at $m = 1/N$. Thus, the optimal solutions for m and v, denoted by m_{opt} and v_{opt}, respectively, are given by:

$$m_{\text{opt}} = 1/N, \tag{45}$$

$$v_{\text{opt}} = \frac{\mathbb{E}[\mathsf{Y}_N]}{1 - m^2_{\text{opt}} N}, \tag{46}$$

where the expression for $\mathbb{E}[\mathsf{Y}_N]$ is given by the following lemma:

Lemma 3. *The mean of Y_N is given by*

$$\mathbb{E}[\mathsf{Y}_N] = 1 - N\left(\frac{\rho^2_{\max} - \rho^2_{\min}}{2} + \frac{2}{\pi}\int_{\rho_{\min}}^{\rho_{\max}}\int_{0}^{\infty} u \ \frac{\text{Im}\{\varphi_{\mathsf{T}^{(N)}(u)}(t)\}}{t} \ \mathrm{d}t \ \mathrm{d}u\right), \tag{47}$$

$$\textit{where } \rho_{\min} = \frac{d^{-2}_{\max}}{d^{-2}_{\max} + (N-1)d^{-2}_{\min}}, \tag{48}$$

$$\rho_{\max} = \frac{d^{-2}_{\min}}{d^{-2}_{\min} + (N-1)d^{-2}_{\max}}, \tag{49}$$

$$\textit{and } \varphi_{\mathsf{T}^{(N)}(u)}(t) = \varphi_{\mathsf{A}_1}((1-u)t)(\varphi_{\mathsf{A}_1}(-ut))^{N-1}. \tag{50}$$

Proof: See Appendix B. ∎

Substituting m_{opt} and v_{opt} in (34), we obtain

$$\mathsf{V}_N = v_{\text{opt}} \mathsf{W}_N. \tag{51}$$

Using Approximation 1, $\mathsf{S}(\underline{\mathsf{R}}^{(N)}, \underline{\Theta}^{(N)})$ can be approximated as follows:

$$\mathsf{S}(\underline{\mathsf{R}}^{(N)}, \underline{\Theta}^{(N)}) \approx \frac{4}{T_{\text{s}} \mathsf{X}_N \mathsf{V}_N}, \tag{52}$$

where V_N is given by (51). We now proceed to derive an approximate expression for the ccdf of $\mathsf{S}(\underline{\mathsf{R}}^{(N)}, \underline{\Theta}^{(N)})$ using (52).

Theorem 1. *The SPEB ccdf, $\overline{F}_{\mathsf{S}_N}(\cdot)$, can be approximated as follows:*

$$\overline{F}_{\mathsf{S}_N}(u) \approx 1 - \mathbb{E}_{\mathsf{X}_N}\left[\overline{F}_{\mathsf{W}_N}\left(\frac{4}{T_{\text{s}} u \mathsf{X}_N v_{\text{opt}}}\right)\right] := \overline{F}_{\mathsf{S}_N,\text{app}}(u), \tag{53}$$

where $\overline{F}_{\mathsf{W}_N}(\cdot)$ is given by (20), v_{opt} by (46) and Lemma 3, and the distribution of X_N by (30).

Proof: From (52), we get

$$\overline{F}_{\mathsf{S}_N}(u) \approx 1 - \mathbb{E}_{\mathsf{X}_N}\left[\overline{F}_{\mathsf{V}_N|\mathsf{X}_N}\left(\frac{4}{T_{\text{s}} u x}\middle| x\right)\right] \tag{54}$$

$$\overset{(a)}{=} 1 - \mathbb{E}_{\mathsf{X}_N}\left[\overline{F}_{\mathsf{W}_N|\mathsf{X}_N}\left(\frac{4}{T_{\text{s}} u x v_{\text{opt}}}\middle| x\right)\right] \tag{55}$$

Algorithm 1 Steps involved in computing $\overline{F}_{\mathsf{S}_N,\mathrm{app}}(.)$

Compute $\mathbb{E}[\mathsf{Y}_N]$ according to (47)
Compute v_{opt} using $\mathbb{E}[\mathsf{Y}_N]$ according to (46)
for each $u > 0$ **do**
  Compute $\overline{F}_{\mathsf{S}_N,\mathrm{app}}(u)$ using (59)-(62)
end for

$$\overset{(b)}{=} 1 - \mathbb{E}_{\mathsf{X}_N}\left[\overline{F}_{\mathsf{W}_N}\left(\frac{4}{T_{\mathrm{s}} u \mathsf{X}_N v_{\mathrm{opt}}}\right)\right] \tag{56}$$

$$:= \overline{F}_{\mathsf{S}_N,\mathrm{app}}(u), \tag{57}$$

where (a) follows from (51), and (b) from the independence of X_N and W_N. ∎

Using (32), $\overline{F}_{\mathsf{S}_N,\mathrm{app}}(\cdot)$ can be expressed as follows:

$$\overline{F}_{\mathsf{S}_N,\mathrm{app}}(u) = 1 - \mathbb{E}_{\mathsf{X}_N}\left[\overline{F}_{\mathsf{W}_N}\left(\frac{4}{T_{\mathrm{s}} u \mathsf{X}_N v_{\mathrm{opt}}}\right)\right]$$
$$= 1 - \left(\int_0^\infty \left[\frac{\mathrm{d}}{\mathrm{d}z}\overline{F}_{\mathsf{W}_N}\left(\frac{4}{T_s u v_{\mathrm{opt}} z}\right)\right]\overline{F}_{\mathsf{X}_N}(z)\mathrm{d}z\right) \tag{58}$$

From (20) and (30), (58) can be expressed as follows:

$$\overline{F}_{\mathsf{S}_N,\mathrm{app}}(u) = 1 - \int_0^\infty \frac{\delta}{uz^2}\left(\frac{N}{2} I_1(z;u,\delta) + \frac{N^2}{4} I_2(z;u,\delta)\right)$$
$$\left(\frac{1}{2} + \frac{1}{\pi}\int_0^\infty \frac{\mathrm{Im}\{\exp(-itz)\varphi_{\mathsf{X}_N}(t)\}}{t}\mathrm{d}t\right)\mathrm{d}z, \tag{59}$$

where $\delta := \dfrac{4}{T_s v_{\mathrm{opt}}}$ (60)

$$I_1(z;u,\delta) := \frac{1}{\sqrt{1-\frac{\delta}{uz}}}\int_0^\infty J_1\left(N\sqrt{1-\frac{\delta}{uz}}y\right)(J_0(y))^N \mathrm{d}y \tag{61}$$

$$I_2(z;u,\delta) := \int_0^\infty \left[J_0\left(N\sqrt{1-\frac{\delta}{uz}}y\right) - J_2\left(N\sqrt{1-\frac{\delta}{uz}}y\right)\right]$$
$$\times\, y(J_0(y))^N \mathrm{d}y \tag{62}$$

The steps involved in computing $\overline{F}_{\mathsf{S}_N,\mathrm{app}}(\cdot)$ are listed in Algorithm 1, where the terms involving integrals can be evaluated numerically using standard software packages. We conclude this section with a few remarks on the results derived in this subsection.

C. Remarks

- Firstly, for the special case when $\underline{\mathsf{R}}^{(N)} = \mathsf{R}\mathbf{1}$, the approximation in (34) reduces to an equality (i.e., $\mathsf{Y}_N = \mathsf{V}_N = \mathsf{W}_N$), with $v = 1$ and $m = 1/N$.
- The quantity V_N in Approximation 1 captures the relationship between $\mathsf{S}(\underline{\mathsf{R}}^{(N)}, \underline{\Theta}^{(N)})$ and the angular geometry of the anchor locations relative to the target, analogous to the manner in which W_N does so for $\mathsf{G}(\mathsf{R}, \underline{\Theta}^{(N)})$. From this perspective, $m_{\mathrm{opt}} = 1/N$ results in V_N being a scaled version of W_N, which is intuitive. Furthermore, the scaling factor v_{opt} can be thought of as a correction term due to SNR heterogeneity that minimizes the error (from a constrained second moment perspective) due to the assumption that $\mathsf{B}_{k,N} \approx m_{\mathrm{opt}}$ for all k.
- Incidentally, we observe that $\mathbb{E}[\mathsf{B}_{k,N}] = 1/N = m_{\mathrm{opt}}$. To see this, $\mathbb{E}[\mathsf{B}_{k,N}]$ can be expressed as follows:

$$\mathbb{E}[\mathsf{B}_{k,N}] = \mathbb{E}_{\mathsf{X}_N}\left[\frac{\mathbb{E}[\mathsf{A}_k|\mathsf{X}_N = x]}{x}\right],\ k = 1, \cdots, N. \tag{63}$$

Since $\underline{\mathsf{A}}^{(N)}$ is a vector of identically distributed random variables, given $\mathsf{X}_N = x$, we have

$$\sum_{k=1}^N \mathbb{E}[A_k|\mathsf{X}_N = x] = \mathbb{E}[\mathsf{X}_N|\mathsf{X}_N = x]$$
$$= x$$
$$= N\mathbb{E}[\mathsf{A}_k|\mathsf{X}_N = x],$$
$$\text{for any } k \in \{1, \cdots, N\} \tag{64}$$

$$\implies \mathbb{E}[\mathsf{A}_k|\mathsf{X}_N = x] = x/N. \tag{65}$$

Substituting (65) in (63), we get

$$\mathbb{E}[\mathsf{B}_{k,N}] = 1/N = m_{\mathrm{opt}}. \tag{66}$$

While, in retrospect, approximating $\mathsf{B}_{k,N}$ by its mean may seem like an obvious choice, the intuition behind $m_{\mathrm{opt}} = 1/N$ as noted in the previous remark and its optimality from a constrained moment matching perspective is not self-evident.
- From the pathloss model assumed in (14), we infer that the term X_N is, in general, proportional to $\sum_{k=1}^N \mathsf{SNR}_k$, the sum SNR across all links. Unlike (14), the pathloss exponent can, in general, be different for each link. In addition, the DP signal often experiences both shadowing and small-scale fading. Hence, SNR_k is typically a complicated function of the distance, R_k, for many propagation environments. Therefore, a closed-form characterization of the distribution of X_N may not be tractable for more advanced channel models and its distribution may need to be approximated by fitting to a known family of distributions.
- The expression for $\overline{F}_{\mathsf{W}_N}(\cdot)$ in (20) holds true only when $\underline{\Theta}^{(N)}$ is an iid uniform random vector over $[0, 2\pi)$. To the best of our knowledge, the distribution of W_N has not been analyzed for any other distribution of $\underline{\Theta}^{(N)}$. Hence, even the distribution of $\mathsf{G}(\mathsf{R}, \underline{\Theta}^{(N)})$, let alone $\mathsf{S}(\underline{\mathsf{R}}^{(N)}, \underline{\Theta}^{(N)})$, is unknown for a large class of point processes. This motivates future work aimed at point processes that are "better" than the BPP (e.g., point processes for which the 99-th percentile of $\mathsf{G}(\mathsf{R}, \underline{\Theta}^{(N)})$ or $\mathsf{S}(\underline{\mathsf{R}}^{(N)}, \underline{\Theta}^{(N)})$ is smaller than the corresponding values for the BPP, say).

In the next section, we present numerical results pertaining to Theorem 1.

IV. Numerical Results

For our simulations, we consider $\overline{F}_{\mathsf{S}_N}(.)$, obtained from 10^6 realizations of (22), $\overline{F}_{\mathsf{S}_N,\mathrm{app}}(.)$ obtained from Theorem 1,

$\overline{F}_{\mathsf{G}_N}(\cdot)$ from (19), and the ccdfs corresponding to the following GDOP-based bounds:

- *Upper and lower bounds to* $\mathsf{S}(\underline{\mathsf{R}}^{(N)}, \underline{\Theta}^{(N)})$*, based on* $\mathsf{G}(\mathsf{R}, \underline{\Theta}^{(N)})$: Let $\mathsf{R}_{(1)}$ and $\mathsf{R}_{(N)}$ denote the distance of the nearest and farthest anchors, respectively. $\mathsf{S}(\underline{\mathsf{R}}^{(N)}, \underline{\Theta}^{(N)})$ can then be bounded as follows:

$$\mathsf{G}(\mathsf{R}_{(1)}, \underline{\Theta}^{(N)}) \leq \mathsf{S}(\underline{\mathsf{R}}^{(N)}, \underline{\Theta}^{(N)}) \leq \mathsf{G}(\mathsf{R}_{(N)}, \underline{\Theta}^{(N)}). \tag{67}$$

As a result, $\overline{F}_{\mathsf{S}_N}(\cdot)$ can be bounded using (19), in the following manner:

$$\overline{F}_{\text{near},N}(u) \leq \overline{F}_{\mathsf{S}_N}(u) \leq \overline{F}_{\text{far},N}(u), \tag{68}$$

where $\overline{F}_{\text{near},N}(u)$ and $\overline{F}_{\text{far},N}(u)$ denote the ccdfs of $\mathsf{G}(\mathsf{R}_{(1)}, \underline{\Theta}^{(N)})$ and $\mathsf{G}(\mathsf{R}_{(N)}, \underline{\Theta}^{(N)})$, respectively, and have the following expressions:

$$\overline{F}_{\text{near},N}(u) = 1 - \mathbb{E}_{\mathsf{R}_{(1)}}\left[\overline{F}_{\mathsf{W}_N}\left(\frac{4\mathsf{R}_{(1)}^2}{T_{\text{s}}Nu}\right)\right] \tag{69}$$

$$\overline{F}_{\text{far},N}(u) = 1 - \mathbb{E}_{\mathsf{R}_{(N)}}\left[\overline{F}_{\mathsf{W}_N}\left(\frac{4\mathsf{R}_{(N)}^2}{T_{\text{s}}Nu}\right)\right], \tag{70}$$

and the ccdfs of $\mathsf{R}_{(1)}$ and $\mathsf{R}_{(N)}$ are given by:

$$\overline{F}_{\mathsf{R}_{(1)}}(r) = \left(\frac{d_{\max}^2 - r^2}{d_{\max}^2 - d_{\min}^2}\right)^N \mathbb{1}(r \in [d_{\min}, d_{\max}]). \tag{71}$$

$$\overline{F}_{\mathsf{R}_{(N)}}(r) = \left[1 - \left(\frac{r^2 - d_{\min}^2}{d_{\max}^2 - d_{\min}^2}\right)^N\right] \mathbb{1}(r \in [d_{\min}, d_{\max}]). \tag{72}$$

For $d_{\min} = 1\text{m}$, the impact of SNR heterogeneity on the outage probability, p_{out}, can be seen in Fig. 3 which plots p_{out} as a function of $d_{\max}$ for an error threshold, $\epsilon_{\text{th}}^{(N)}$, corresponding to a 1% outage probability when N anchors are present and $d_{\max} = d_{\min} = 1\text{m}$ (i.e., the homogeneous SNR case) . Naturally, $p_{\text{out}} = \overline{F}_{\mathsf{S}_N}(\epsilon_{\text{th}}^{(N)}) \geq \mathbb{P}(\mathsf{G}(d_{\min}, \underline{\Theta}^{(N)}) > \epsilon_{\text{th}}^{(N)}) = 0.01$ since $\mathsf{S}(\underline{\mathsf{R}}^{(N)}, \underline{\Theta}^{(N)}) \geq \mathsf{G}(d_{\min}, \underline{\Theta}^{(N)})$, but even for $d_{\max}$ as small as 4m, p_{out} increases by nearly an order of magnitude to approximately 0.1 for $N = 3$ and by two orders of magnitude for $N \geq 7$. This highlights the close relationship between SNR heterogeneity and p_{out}, and by extension, the SPEB distribution as well.

For $d_{\min} = 1\text{m}$ and $d_{\max} = 10\text{m}$, which is a reasonable assumption for the link distances encountered in indoor applications, the ccdf curves are plotted as a function of the SPEB, scaled by the term T_{s}, in Fig. 4 for $N \in \{3, \cdots, 8\}$. For all the values of N considered, it can be seen that $\overline{F}_{\mathsf{S}_N,\text{app}}$ is accurate at estimating $\overline{F}_{\mathsf{S}_N}(\cdot)$. In particular, the accurate estimation of the tail of $\overline{F}_{\mathsf{S}_N}(\cdot)$ is especially important from a design perspective, as it captures the *outage regime*. To quantify the accuracy of $\overline{F}_{\mathsf{S}_N,\text{app}}(\cdot)$ in this regime, we plot p_{out} as a function of $d_{\max}$ with $d_{\min} = 1\text{m}$ in Fig. 5 for an error threshold, $\epsilon_N(d_{\max})$, corresponding to a 1% outage probability (i.e., $\overline{F}_{\mathsf{S}_N}(\epsilon_N(d_{\max})) = 0.01$). Consistent with the observation from Fig. 4, $\overline{F}_{\mathsf{S}_N,\text{app}}(\epsilon_N(d_{\max})) \approx 0.01$ across all values of N and $d_{\max}$, which implies that for a given value of the outage threshold, $\overline{F}_{\mathsf{S}_N,\text{app}}(\cdot)$ can be used to estimate the minimum number of anchors, N, needed for the outage probability to be at most 1%. In contrast, the GDOP based approximation and bounds become progressively inaccurate with increasing N and $d_{\max}$. This further highlights the importance of distance-dependent SNR heterogeneity on the SPEB distribution.

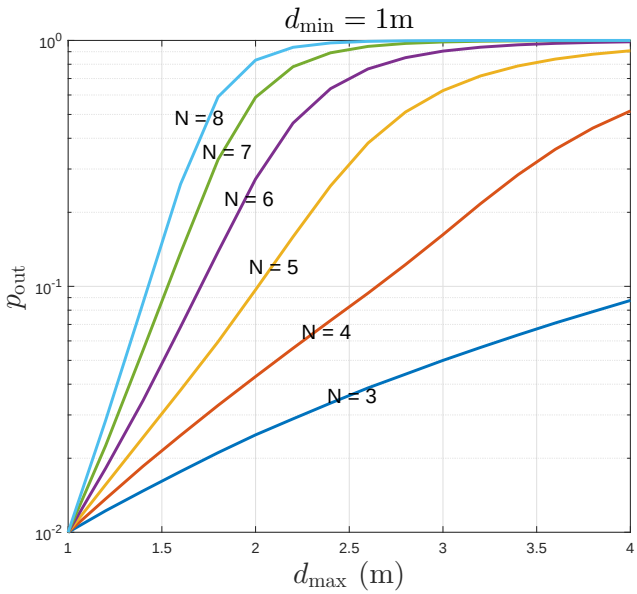

Fig. 3: The error threshold, $\epsilon_{\text{th}}^{(N)}$, corresponds to 1% outage probability when $d_{\max} = d_{\min} = 1\text{m}$ (i.e., $\mathbb{P}(\mathsf{G}(d_{\min}, \underline{\Theta}^{(N)}) > \epsilon_{\text{th}}^{(N)}) = 0.01$).

V. Conclusion

In this paper, we set out to characterize the impact of distance-based SNR heterogeneity on the error performance of ToA-based localization using the SPEB metric, $\mathsf{S}(\underline{\mathsf{R}}^{(N)}, \underline{\Theta}^{(N)})$. From the perspective of a given target, we considered an ensemble of anchor locations modeled as a BPP over an annular region centered at the target and assumed a distance-dependent inverse-square law pathloss model to capture the SNR heterogeneity. For this setup, $\mathsf{S}(\underline{\mathsf{R}}^{(N)}, \underline{\Theta}^{(N)})$ was shown to be a tightly coupled function of the anchor distances $(\underline{\mathsf{R}}^{(N)})$ and angular positions $(\underline{\Theta}^{(N)})$ and as a result, its ccdf, $\overline{F}_{\mathsf{S}_N}(\cdot)$, was difficult to characterize in closed-form. Hence, we formulated an approximation for $\mathsf{S}(\underline{\mathsf{R}}^{(N)}, \underline{\Theta}^{(N)})$, where the coupling between $\underline{\mathsf{R}}^{(N)}$ and $\underline{\Theta}^{(N)}$ was removed by constrained moment matching, which enabled us to derive a closed-form approximation, $\overline{F}_{\mathsf{S}_N,\text{app}}(\cdot)$, of $\overline{F}_{\mathsf{S}_N}(\cdot)$. Through simulations, we observed that $\overline{F}_{\mathsf{S}_N,\text{app}}(\cdot)$ was accurate at estimating $\overline{F}_{\mathsf{S}_N}(\cdot)$, especially at the tail which corresponds to the outage regime. In particular, it was observed that for distances up to 10m, $\overline{F}_{\mathsf{S}_N,\text{app}}(\cdot)$ can be used to determine the minimum number of anchors needed to guarantee an outage probability of at most 1% for a given outage threshold, ϵ_{th}.

The accuracy of $\overline{F}_{\mathsf{S}_N,\text{app}}(\cdot)$ motivates future work where the MSE can be approximated (upto a constant of proportionality)

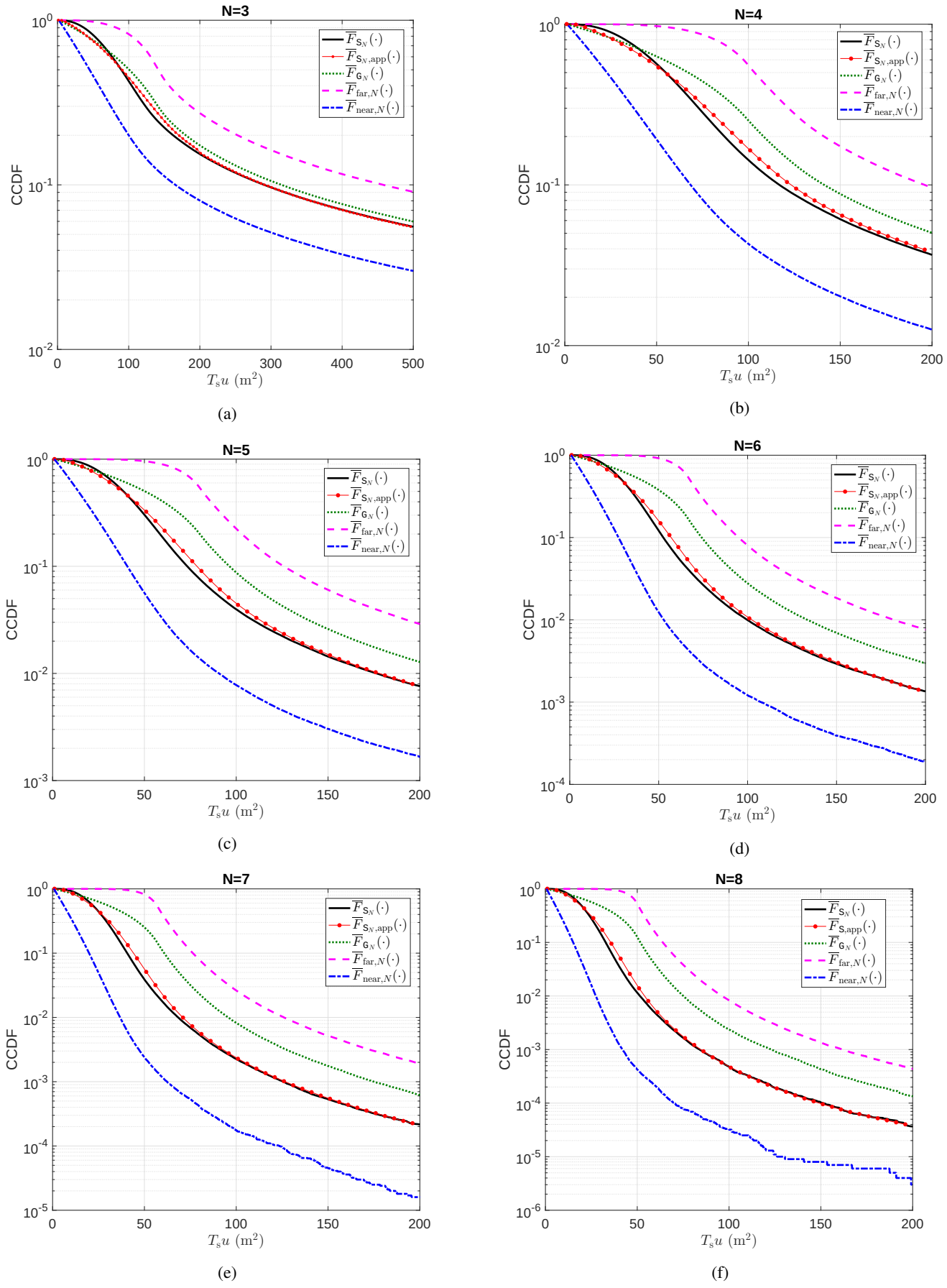

Fig. 4: $\overline{F}_{\mathsf{S}_N,\mathrm{app}}(.)$ accurately estimates $\overline{F}_{\mathsf{S}_N}(\cdot)$ since it captures the SNR heterogeneity across multiple links induced primarily by the anchors being at different distances from the target ($d_{\min} = 1\mathrm{m}$ and $d_{\max} = 10\mathrm{m}$).

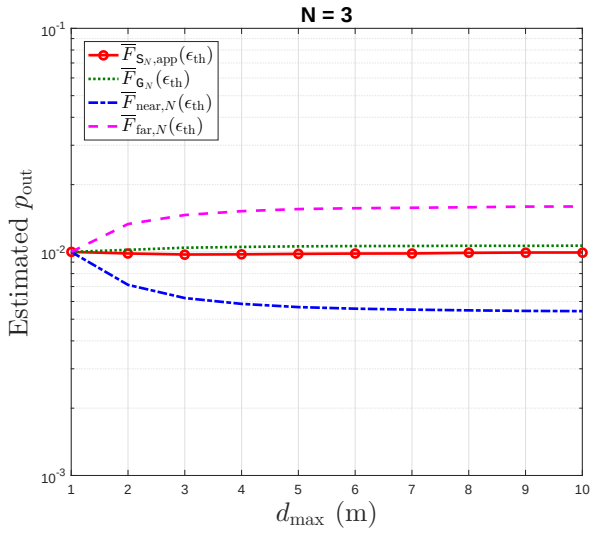

(a)

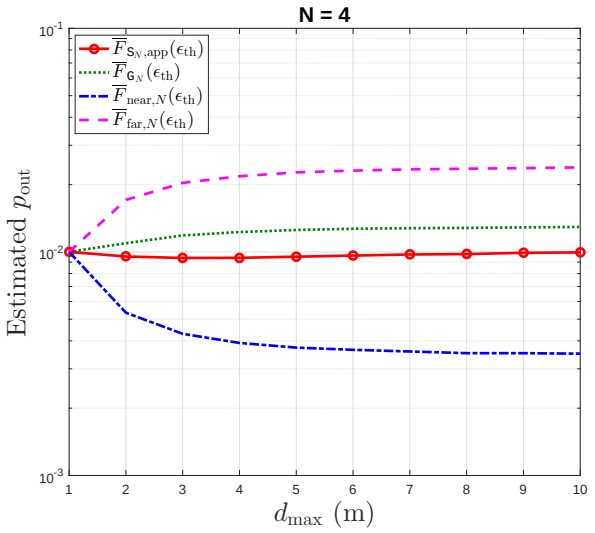

(b)

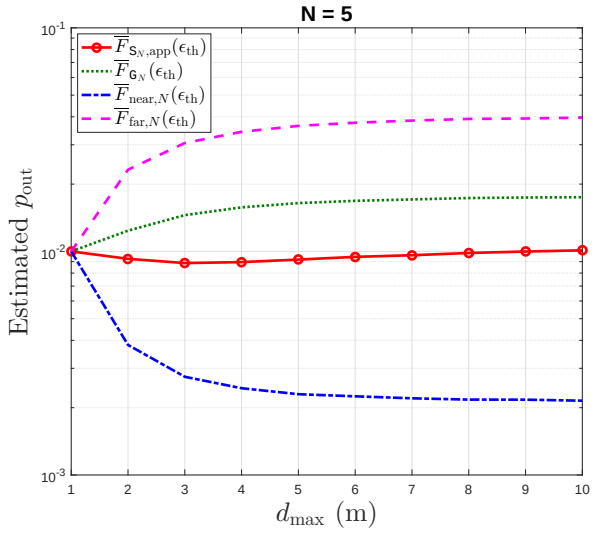

(c)

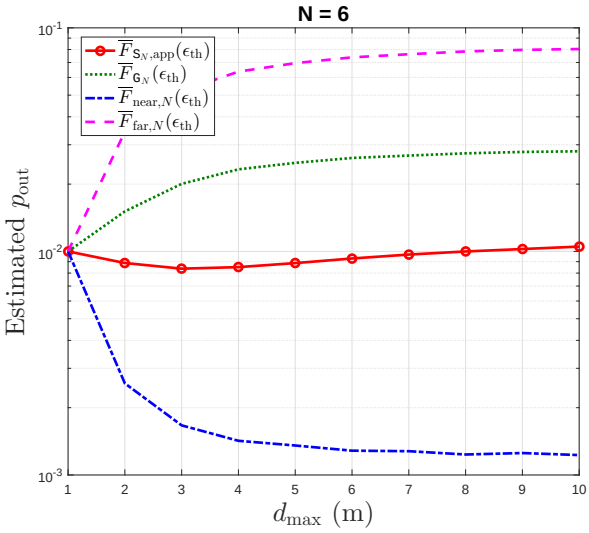

(d)

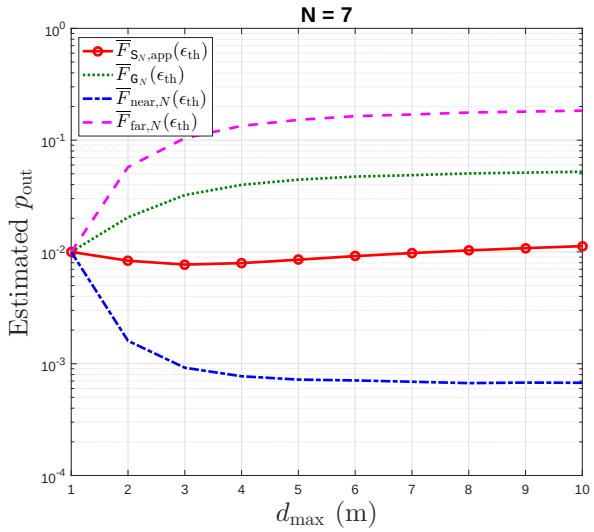

(e)

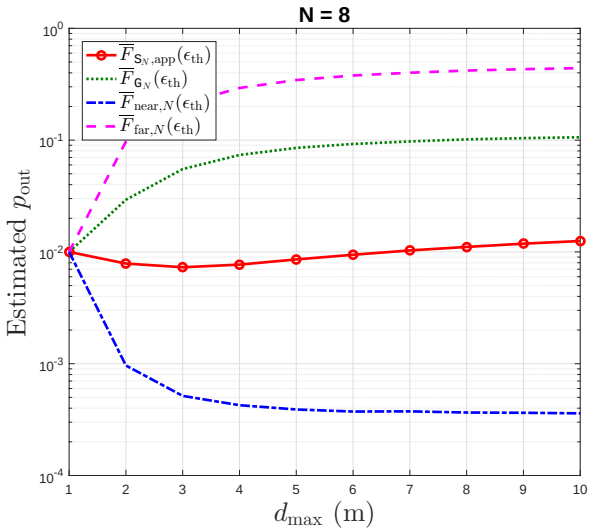

(f)

Fig. 5: For a given threshold, ϵ_{th}, $\overline{F}_{\mathtt{S}_N,\text{app}}(\cdot)$ can be used to determine the value of N such that the outage probability is at most 1% ($d_{\min} = 1\text{m}$).

as follows,

$$\mathrm{MSE} \approx v_c \left(\mathsf{W}_N \sum_{k=1}^{N} \mathsf{SNR}_k \right)^{-1}, \tag{73}$$

where the sum SNR captures the radial component (see Section III-C, bullet point 4) and W_N the azimuthal component, while v_c is a correction term that can be optimized to minimize the errors from assuming such a decoupled structure for the MSE. In this paper, we derived an expression for v_c when the SNR decays with distance according to an inverse-square law and the anchors are distributed according to a BPP, but other cases of practical interest that could be studied under this framework are:

- Varying path loss exponents for different links,
- Links affected by shadowing and small-scale fading
- Anchor deployments that are "better" than the BPP (e.g., point processes for which the 99-th percentile of $\mathsf{S}(\underline{\mathsf{R}}^{(N)}, \underline{\Theta}^{(N)})$ is smaller than the corresponding value for the BPP, say).

APPENDIX

A. Proof of Lemma 2

Since $\underline{\mathsf{A}}^{(N)}$ is an iid random vector, the characteristic function of $\mathsf{X}_N = \mathsf{A}_1 + \cdots + \mathsf{A}_N$ is given by

$$\varphi_{\mathsf{X}_N}(t) = (\varphi_{\mathsf{A}_1}(t))^N \tag{74}$$

From (24) and (21), the pdf of A_1 can be expressed as follows:

$$f_{\mathsf{A}_1}(a) = (1/2)a^{-3/2} f_{\mathsf{R}}(a^{-1/2}) \tag{75}$$

$$\begin{aligned} \therefore\ \varphi_{\mathsf{A}_1}(t) &= \mathbb{E}[\exp(it\mathsf{A}_1)] \\ &= \int_{-\infty}^{\infty} \cos(ta) f_{\mathsf{A}_1}(a)\ \mathrm{d}a + i \int_{-\infty}^{\infty} \sin(ta) f_{\mathsf{A}_1}(a)\ \mathrm{d}a \\ &= I_{\mathrm{c}}(t; d_{\min}, d_{\max}) + i I_{\mathrm{s}}(t; d_{\min}, d_{\max}), \end{aligned} \tag{76}$$

$$\text{where } I_{\mathrm{c}}(t; d_{\min}, d_{\max}) := \int_{-\infty}^{\infty} \cos(ta) f_{\mathsf{A}_1}(a)\ \mathrm{d}a, \tag{77}$$

$$\text{and } I_{\mathrm{s}}(t; d_{\min}, d_{\max}) := \int_{-\infty}^{\infty} \sin(ta) f_{\mathsf{A}_1}(a)\ \mathrm{d}a. \tag{78}$$

Integrating (77) and (78) by parts, we get

$$\begin{aligned} I_{\mathrm{c}}(t; d_{\min}, d_{\max}) &= \left(\frac{1}{d_{\max}^2 - d_{\min}^2} \right) \left[d_{\max}^2 \cos\left(\frac{t}{d_{\max}^2} \right) \right. \\ &\left. - d_{\min}^2 \cos\left(\frac{t}{d_{\min}^2} \right) - t\mathrm{Si}\left(\frac{t}{d_{\min}^2} \right) + t\mathrm{Si}\left(\frac{t}{d_{\max}^2} \right) \right], \end{aligned} \tag{79}$$

$$\begin{aligned} I_{\mathrm{s}}(t; d_{\min}, d_{\max}) &= \left(\frac{1}{d_{\max}^2 - d_{\min}^2} \right) \left[d_{\max}^2 \sin\left(\frac{t}{d_{\max}^2} \right) \right. \\ &\left. - d_{\min}^2 \sin\left(\frac{t}{d_{\min}^2} \right) - t\mathrm{Ci}\left(\frac{t}{d_{\max}^2} \right) + t\mathrm{Ci}\left(\frac{t}{d_{\min}^2} \right) \right], \end{aligned} \tag{80}$$

where $\mathrm{Si}(\cdot)$ and $\mathrm{Ci}(\cdot)$ are given by (1) and (2), respectively. Combining (76), (79), (80) and (3), we get

$$\begin{aligned} \varphi_{\mathsf{A}_1}(t) &= \left(\frac{1}{d_{\max}^2 - d_{\min}^2} \right) \left[d_{\max}^2 \exp\left(i \frac{t}{d_{\max^2}} \right) \right. \\ &\left. - d_{\min}^2 \exp\left(i \frac{t}{d_{\min^2}} \right) + t\mathrm{H}\left(\frac{t}{d_{\max}^2} \right) - t\mathrm{H}\left(\frac{t}{d_{\min}^2} \right) \right]. \end{aligned} \tag{81}$$

■

B. Proof of Lemma 3

$\mathsf{B}_{1,N}, \cdots, \mathsf{B}_{N,N}$ form a collection of identically distributed, but *not independent*, random variables. In addition, Θ_j and $\mathsf{B}_{k,N}$ are also independent random variables, for any j, k. Hence, from (25), we obtain

$$\mathbb{E}[\mathsf{Y}_N] = 1 - N\mathbb{E}[\mathsf{B}_{1,N}^2], \tag{82}$$

For a fixed $b \in \mathbb{R}$, the function $x/(x+b)$ is increasing in x. Hence, from (26), it follows that $\mathsf{B}_{1,N}$ is increasing in A_1, for fixed $\mathsf{A}_2, \cdots, \mathsf{A}_N$. As a result, $\mathsf{B}_{1,N} \in [\rho_{\min}, \rho_{\max}]$, where

$$\rho_{\min} = \frac{d_{\max}^{-2}}{d_{\max}^{-2} + (N-1)d_{\min}^{-2}}, \tag{83}$$

$$\rho_{\max} = \frac{d_{\min}^{-2}}{d_{\min}^{-2} + (N-1)d_{\max}^{-2}}. \tag{84}$$

As $\mathsf{B}_{k,N}$ is non-negative for all k, $\mathbb{E}[\mathsf{B}_{1,N}^2]$ can be expressed as follows:

$$\mathbb{E}[\mathsf{B}_{1,N}^2] = 2 \int_{\rho_{\min}}^{\rho_{\max}} u\ \overline{F}_{\mathsf{B}_{1,N}}(u) \mathrm{d}u. \tag{85}$$

From (26), $\overline{F}_{\mathsf{B}_{1,N}}(u)$ can be expressed as follows:

$$\overline{F}_{\mathsf{B}_{1,N}}(u) = \overline{F}_{\mathsf{T}^{(N)}(u)}(0), \tag{86}$$

$$\text{where } \mathsf{T}^{(N)}(u) = \mathsf{A}_1(1-u) - u\sum_{j=2}^{N} \mathsf{A}_j \tag{87}$$

Since $\underline{\mathsf{A}}^{(N)}$ is an iid random vector, the characteristic function of $\mathsf{T}^{(N)}(u)$ has the following expression:

$$\varphi_{\mathsf{T}^{(N)}(u)}(t) = \varphi_{\mathsf{A}_1}((1-u)t)(\varphi_{\mathsf{A}_1}(-ut))^{N-1}. \tag{88}$$

Similar to (30), $\overline{F}_{\mathsf{T}^{(N)}(u)}(0)$ can be evaluated from $\varphi_{\mathsf{T}_1^{(N)}(u)}(t)$, as follows:

$$\overline{F}_{\mathsf{T}^{(N)}(u)}(0) = \frac{1}{2} + \frac{1}{\pi} \int_0^{\infty} \frac{\mathrm{Im}\{\varphi_{\mathsf{T}^{(N)}(u)}(t)\}}{t}\ \mathrm{d}t. \tag{89}$$

Combining (82)-(89), we get

$$\begin{aligned} \mathbb{E}[\mathsf{Y}_N] = 1 - N \left(\frac{\rho_{\max}^2 - \rho_{\min}^2}{2} \right. \\ \left. + \frac{2}{\pi} \int_{\rho_{\min}}^{\rho_{\max}} \int_0^{\infty} u\ \frac{\mathrm{Im}\{\varphi_{\mathsf{T}^{(N)}(u)}(t)\}}{t}\ \mathrm{d}t\ \mathrm{d}u \right). \end{aligned} \tag{90}$$

■

REFERENCES

[1] D. Cui, J. Xue, and N. Zheng, "Real-time global localization of robotic cars in lane level via lane marking detection and shape registration," *IEEE Trans. Intell. Transp. Syst.*, vol. 17, no. 4, pp. 1039–1050, Apr. 2016.

[2] G. Cardone, L. Foschini, P. Bellavista, A. Corradi, C. Borcea, M. Talasila, and R. Curtmola, "Fostering ParticipAction in Smart Cities: A geo-social crowdsensing platform," *IEEE Commun. Mag.*, vol. 51, no. 6, pp. 112–119, Jun. 2013.

[3] S. Steineger, M. Neun, A. Edwardes, and B. Lenz, "Foundations of location based services," 2006. [Online]. Available: http://www.e-cartouche.ch/content_reg/cartouche/LBSbasics/en/text/LBSbasics.pdf

[4] K. Clark, "Virtual reality roller coasters are here (and everywhere)," *IEEE Spectr.*, Mar. 2016. [Online]. Available: https://spectrum.ieee.org/geek-life/reviews/virtual-reality-roller-coasters-are-here-and-everywhere

[5] S. Gezici, Z. Tian, G. Giannakis, H. Kobayashi, A. F. Molisch, H. Poor, and Z. Sahinoglu, "Localization via ultra-wideband radios: a look at positioning aspects for future sensor networks," *IEEE Signal Process. Mag.*, vol. 22, no. 4, pp. 70–84, Jul. 2005.

[6] "Wireless E911 location accuracy requirements," Federal Communications Commission, Tech. Rep. PS Docket No. 07-114, Jan. 2015.

[7] D. B. Jourdan, D. Dardari, and M. Z. Win, "Position error bound for UWB localization in dense cluttered environments," *IEEE Trans. Aerosp. Electron. Syst.*, vol. 44, no. 2, pp. 613–628, Apr. 2008.

[8] Y. Shen and M. Win, "Fundamental Limits of Wideband Localization; Part I: A General Framework," *IEEE Trans. Inf. Theory*, vol. 56, no. 10, pp. 4956 –4980, Oct. 2010.

[9] D. Stoyan, S. N. Chiu, W. S. Kendall, and J. Mecke, *Stochastic geometry and its applications*, 3rd ed. Wiley, 2013.

[10] C. E. O'Lone and R. M. Buehrer, "An analysis of the convex hull's impact on localization performance," in *Proc. of IEEE/ION Position, Location and Navigation Symposium (PLANS)*, Apr. 2016, pp. 519–526.

[11] Y. Shen, H. Wymeersch, and M. Win, "Fundamental Limits of Wideband Localization; Part II: Cooperative Networks," *IEEE Trans. Inf. Theory*, vol. 56, no. 10, pp. 4981 –5000, Oct. 2010.

[12] B. Huang, T. Li, B. D. O. Anderson, and C. Yu, "On the performance limit of single-hop toa localization," in *Proc. of the 12th Intl. Conf. on Control Automation Robotics Vision (ICARCV)*, Dec. 2012, pp. 42–46.

[13] J. Schloemann, H. S. Dhillon, and R. M. Buehrer, "A tractable metric for evaluating base station geometries in cellular network localization," *IEEE Wireless Commun. Lett.*, vol. 5, no. 2, pp. 140–143, Apr. 2016.

[14] C. E. O'Lone, H. S. Dhillon, and R. M. Buehrer, "A statistical characterization of localization performance in wireless networks," *IEEE Trans. Wireless Commun.*, vol. 17, no. 9, Sep. 2018.

[15] F. Zhou and Y. Shen, "On the outage probability of localization in randomly deployed wireless networks," *IEEE Commun. Lett.*, vol. 21, no. 4, pp. 901–904, Apr. 2017.

[16] J. Schloemann, H. S. Dhillon, and R. M. Buehrer, "Towards a tractable analysis of localization fundamentals in cellular networks," *IEEE Trans. Wireless Commun.*, vol. 15, no. 3, pp. 1768–1782, Mar. 2016.

[17] T. Bhandari, H. S. Dhillon, and R. M. Buehrer, "The impact of proximate base station measurements on localizability in cellular systems," in *Proc. of IEEE Intl. Workshop on Signal Process. Advances in Wireless Commun. (SPAWC)*, Jul. 2016.

[18] J. Schloemann, H. S. Dhillon, and R. M. Buehrer, "A tractable analysis of the improvement in unique localizability through collaboration," *IEEE Trans. Wireless Commun.*, vol. 15, no. 6, pp. 3934–3948, Jun. 2016.

[19] S. Aditya, H. S. Dhillon, A. F. Molisch, and H. Behairy, "Asymptotic blind-spot analysis of localization networks under correlated blocking using a poisson line process," *IEEE Wireless Commun. Lett.*, vol. 6, no. 5, pp. 654–657, Oct. 2017.

[20] ——, "A tractable analysis of the blind-spot probability in localization networks under correlated blocking," *IEEE Trans. Wireless Commun.*, 2017, under review. [Online]. Available: https://arxiv.org/abs/1801.08560

[21] A. F. Molisch, *Wireless Communications*, 2nd ed. Wiley, 2011.

[22] J. Shen, A. F. Molisch, and J. Salmi, "Accurate Passive Location Estimation Using TOA Measurements," *IEEE Transactions on Wireless Communications*, vol. 11, no. 6, pp. 2182–2192, Jun. 2012.

[23] P. Meissner, E. Leitinger, and K. Witrisal, "UWB for robust indoor tracking: Weighting of multipath components for efficient estimation," *IEEE Wireless Commun. Lett.*, vol. 3, no. 5, pp. 501–504, Oct. 2014.

[24] E. Leitinger, M. Froehle, P. Meissner, and K. Witrisal, "Multipath-assisted maximum-likelihood indoor positioning using UWB signals," in *Proc. of IEEE ICC Workshop on Advanced Network Localization and Navigation (ANLN)*, Jun. 2014, pp. 170–175.

[25] P. Meissner, E. Leitinger, M. Lafer, and K. Witrisal, "Real-time demonstration of multipath-assisted indoor navigation and tracking (MINT)," in *Proc. of IEEE ICC Workshop on Advanced Network Localization and Navigation (ANLN)*, Jun. 2014, pp. 144–149.

[26] D. Torrieri, "Statistical theory of passive location systems," *IEEE Trans. Aerosp. Electron. Syst.*, vol. AES-20, no. 2, pp. 183–198, Mar. 1984.

[27] Y. Shen, W. Dai, and M. Z. Win, "Power optimization for network localization," *IEEE/ACM Trans. Netw.*, vol. 22, no. 4, pp. 1337–1350, Aug. 2014.

[28] W. Dai, Y. Shen, and M. Z. Win, "A computational geometry framework for efficient network localization," *IEEE Trans. Inf. Theory*, vol. 64, no. 2, pp. 1317–1339, Feb. 2018.

[29] J. Gil-Pelaez, "Note on the inversion theorem," *Biometrika*, vol. 38, Dec. 1951.